

# EVALUATION OF PERFORMANCE OF INTEGRATING SPHERES FOR INDIRECT EMITTANCE MEASUREMENT

Alexander Prokhorov, Sergey Mekhontsev, and Leonard Hanssen

National Institute for Standards and Technology, Gaithersburg, MD, USA

## ABSTRACT

Integrating sphere reflectometers are used in the majority of instruments used for spectral reflectance measurements of non-specular (scattering) samples. Knowledge of directional-hemispherical spectral reflectance (and transmittance, in the case of semi-transparent samples) allows one to derive the spectral directional emittance, which is of considerable practical interest for numerous heat transfer and pyrometric applications. The indirect method of emittance measurement is commonly used in cases of low emitted flux such as for samples near or below room temperature. For direct emittance measurement facilities, the indirect method has also been used for accurate non-contact measurement of sample temperature. Along with a number of advantages for reflectance and emittance measurement, integrating spheres possess a considerable number of potential sources of error relating to the characteristics of the sphere and their deviation from ideal behavior. This paper describes an evaluation of the effects of sphere related error sources on a sphere reflectometer's performance by means of a computational model. This effort was undertaken in the framework of a current NIST project to build a facility employing indirect measurements of spectral directional emittance. A description of the modeling program and its assumptions are given. Examples of modeling results for several materials and sphere parameters (such as the wall reflectance and degree of wall coating specularity) and their effects on emittance values are presented and discussed. A discussion of the developed techniques and conclusions as well as the prospects of their practical application to design optimization and uncertainty evaluation of integrating sphere reflectometers and emissometers is presented.

## 1. INTRODUCTION

Integrating spheres are commonly used for spectral reflectance measurements of non-specular (scattering) samples. For opaque materials, the directional emittance can be derived from the directional-hemispherical (or hemispherical-directional) reflectance (indirect method). For transparent materials an additional measurement of directional-hemispherical transmittance is needed [1]. The indirect method employing an integrating sphere is especially useful for cases of low emitted flux such as near or below room temperature. For direct emittance measurement, the indirect method has also been used in a supplementary role in a non-contact determination of sample temperature [2].

Integrating spheres provide a number of advantages for reflectance and emittance measurement. Similarly, however, a number of potential sources of error relating to the characteristics of the sphere and their deviation from ideal behavior can contribute to error in the reflectance, emittance, and temperature measurement results [3]. A useful approach to evaluation of the effects of these error sources is to construct a computational model for the sphere and evaluate its performance for realistic parameter values and various types of samples.

Such a modeling effort was undertaken in support of the current NIST project to develop a spectral directional emittance characterization facility [4], which will employ an integrating sphere reflectometer. While the simulation model is applicable for sphere reflectometers of different geometries, we will limit ourselves to the geometry selected for our emittance measurement system, as described below.

## 2. OBJECTIVES OF WORK

The main objectives of the present work were to develop the method and software for numerical modeling of integrating sphere radiation characteristics, and use this software code to optimize the design and to correct for systematic and predictable effects.

Let us first analyze the assumptions implied by the measurement concept. For an ideal reflectometer, the sample spectral hemispherical-conical reflectance factor  $R_1$  at temperature  $T_1$  and for wavelength  $\lambda$  in the conical solid angle  $\Omega$  can be found from:

$$\frac{R_1(\lambda, 2\pi \rightarrow \Omega, T_1)}{R_2(\lambda, 2\pi \rightarrow \Omega, T_2)} = \frac{V_1}{V_2}, \quad (1)$$

where  $V$  is the detector reading, and subscripts 1 and 2 denote sample and reference, respectively. For a small solid angle  $\Omega$  and samples with a smooth bi-directional reflectance distribution function (BRDF) we can replace the hemispherical-conical spectral reflectance factor  $R(\lambda, 2\pi \rightarrow \Omega, T)$  with the hemispherical-directional one  $R(\lambda, 2\pi \rightarrow \bar{\omega}, T)$ , where the direction  $\bar{\omega}$  coincides with the axis of the conical solid angle  $\Omega$  and in the notation  $a \rightarrow b$ ,  $a$  and  $b$  represent the illumination and collection geometries, respectively. According to the reciprocity theorem, the hemispherical-directional reflectance factor  $R_1(\lambda, 2\pi \rightarrow \bar{\omega}, T_1)$  is equal to the directional-hemispherical reflectance  $\rho_1(\lambda, \bar{\omega} \rightarrow 2\pi, T_1)$ . For an opaque sample, according to the energy conservation law, the directional spectral absorptance  $\alpha_1(\lambda, \bar{\omega}, T_1)$  can be obtained from

$$\alpha_1(\lambda, \bar{\omega}, T_1) = 1 - \rho_1(\lambda, \bar{\omega} \rightarrow 2\pi, T_1). \quad (2)$$

Kirchhoff's law allows us to replace the directional spectral absorptance with the directional spectral emittance  $\varepsilon_1(\lambda, \bar{\omega}, T_1)$  and obtain, taking into account (1) and (2) in terms of known and measured quantities,

$$\varepsilon_1(\lambda, \bar{\omega}, T_1) = 1 - \rho_2(\lambda, \bar{\omega} \rightarrow 2\pi, T_1) \frac{V_1(\lambda)}{V_2(\lambda)}. \quad (3)$$

Application of the reciprocity theorem requires uniform and identical hemispherical illumination of the sample and reference. Hence, the first objective of our work is to model the distribution of the radiance over the hemisphere above the sample center and the influence of its non-uniformity on the measured sample reflectance. Another objective is to evaluate the effects of sample and sphere wall BRDF on the measured reflectance.

Most existing analytical and numerical methods do not allow accurate treatment of the effects of the sphere wall's specularly, which could be vital for IR applications where all coatings exhibit some measurable degree of specularly. The Monte Carlo method, based on the stochastic treatment of interactions of optical radiation with matter, is becoming widely applied to optical radiation transfer analysis, including numerical modeling of integrating spheres [5-8]. This method, having no fundamental restrictions either on system geometry or BRDF of surfaces, has been chosen for the numerical modeling described herein.

### 3. REFLECTOMETER MODEL AND PROGRAM IMPLEMENTATION FEATURES

In this paper the sphere modeling is treated within the framework of geometrical (ray) optics. We assume that a light source emits unpolarized radiation, or it is depolarized after multiple reflections inside the integrating sphere. The modeled system (Figure 1) is formed by the internal surface of the sphere, a flat light source (s), two flat baffles (b), and symmetrically arranged holders (h) with the sample (1) and the reference (2). The sample and reference are viewed by a detector (a). The letters and numbers in parentheses identify each sphere element for specification of their dimensions in Section 4.

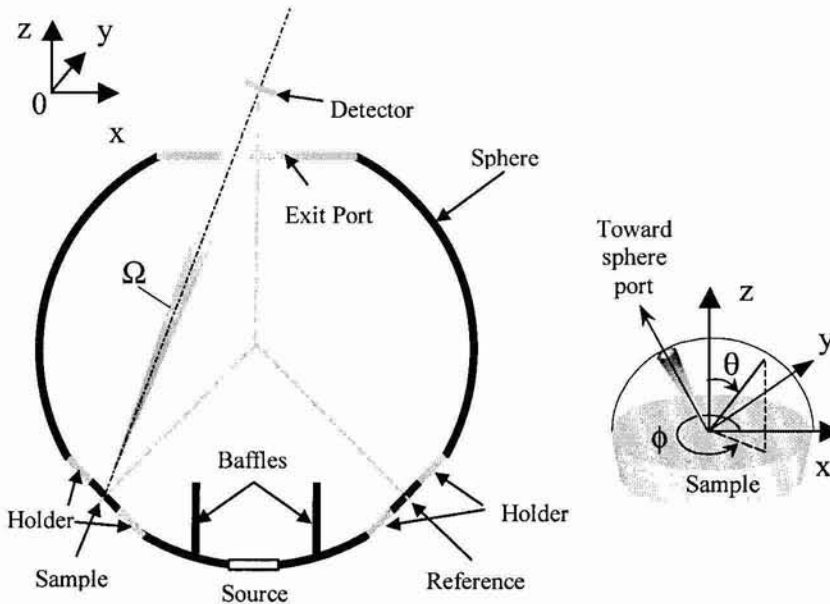


**Figure 1.** Computational model of the integrating sphere and the local spherical coordinate system linked to the sample center. The subscripts are defined in the text.

For elements of the integrating sphere, the specular-diffuse model of reflection with arbitrary dependencies of specular and diffuse components on incident angle has been used. Due to limitations of space, only the uniform specular-diffuse model of reflection is presented, according to which both components do not depend on incident angle. Following Ref. [5], we will characterize each surface by a value of specularity:

$$S = \rho_s / (\rho_s + \rho_d) = \rho_s / \rho, \quad (4)$$

where  $\rho_s$  and  $\rho_d$  are the specular and diffuse components of reflectance; and  $\rho$  is their sum.

The source is assumed to be spatially uniform with angular distribution of radiant intensity defined as

$$I(\theta) = \frac{\nu + 1}{2\pi} I(0) \cos^\nu \theta, \quad (5)$$

where  $\theta$  is the angle between the direction of observation and the normal to the source surface.

The limited scope of this paper does not permit a full description of the developed Monte-Carlo ray tracing technique, which will be the subject of another publication to follow in the near future.

The main problem encountered in numerical modeling of integrating spheres is the time required to perform the simulations. For instance, the requisite very large number of successive reflections,  $M$ , which can be evaluated by the formula:

$$M = \text{Ent} \left( \frac{\ln \gamma}{\ln \rho} \right), \quad (6)$$

where  $\rho$  is the sphere wall reflectance,  $\gamma$  is an allowable relative uncertainty of the radiance due to the neglect of high-order reflections, and  $\text{Ent}(x)$  is the integer part of  $x$ . For example, if we need to compute the radiance of the integrating sphere wall with  $\gamma = 10^{-3}$  and wall reflectance  $\rho = 0.95$ , we should take into account not less than 135 successive reflections. Another cause of slow convergence of computations, in our particular case, is the relatively small size of the source. It was found necessary to trace at least  $1 \cdot 10^7$  rays to achieve a 0.1% level of the radiance standard deviation.

#### 4. RESULTS OF NUMERICAL EXPERIMENTS

The geometrical parameters of the modeled sphere as defined in Figure 1 are the following:  $r = 150$  mm;  $r_a = 26.4$  mm;  $r_{1h} = r_{2h} = 25$  mm;  $r_{1s} = r_{2s} = 9$  mm;  $r_s = 5$  mm;  $\beta = 17^\circ$ ;  $z_0 = 147.6$  mm;  $z_a = 225.8$  mm;  $z_b = 139.9$  mm;  $x_b = 7$  mm. For both holders  $\rho_{1h} = \rho_{2h} = 0.99$ ;  $S_{1h} = S_{2h} = 1$ .

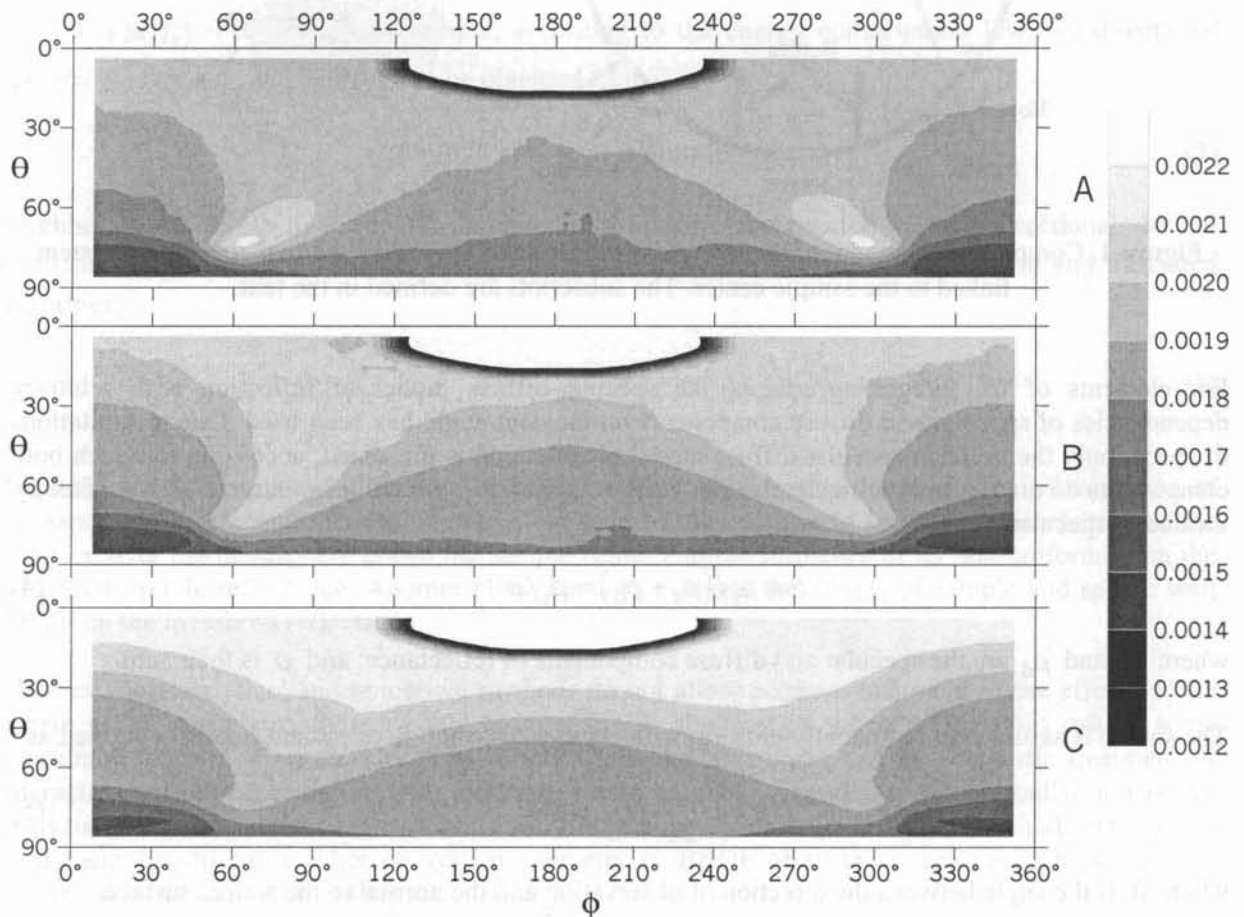


**Figure 2.** Angular distributions of relative radiance of light incident onto sample center for various angular distributions of light source radiant intensity. A:  $v = 0.5$ ; B:  $v = 1$ ; C:  $v = 2$  (See Eq. (5)). The sphere and baffles reflectance is 0.9, with specularity 0.

In Figure 2, maps of the computed hemispherical distributions of relative radiance for light incident onto the sample center, for sources characterized by different indicatrices (power of cosine in Eq. (5),  $\nu = 0.5, 1,$  and  $2$ ) are shown. The white elliptical region near the top in each map corresponds to the conical solid angle subtended by the exit port of the sphere (refer to Figure 1). A small degree of smoothing is applied which results in the gradient at the edge of the exit port. The darkest region near ( $\theta = 90^\circ, \phi = 0^\circ/360^\circ$ ) corresponds to the direction of the center of the baffle. For  $\nu = 0.5$  and  $2$  the non-uniformity of the distribution approaches 25% compared to 15% for the Lambertian radiator case ( $\nu = 1$ ). Additional studies show that the non-uniformity decreases with increasing sphere reflectance. And for the Lambertian radiator, the distribution uniformity is affected mainly by the height of the baffles.

Figure 3 depicts the hemispherical distribution of radiance incident on the sample center for sphere and baffles reflectance 0.95 and two values of specularity. At  $S = 0.2$  (Figure 3A) the series of valleys on the surface correspond to images of the exit port after several reflections. A small peak under the exit port corresponds to the fifth reflection of the light source. At  $S = 0.4$  (Figure 3B), the pattern becomes more apparent with the small peaks corresponding to higher order reflections.

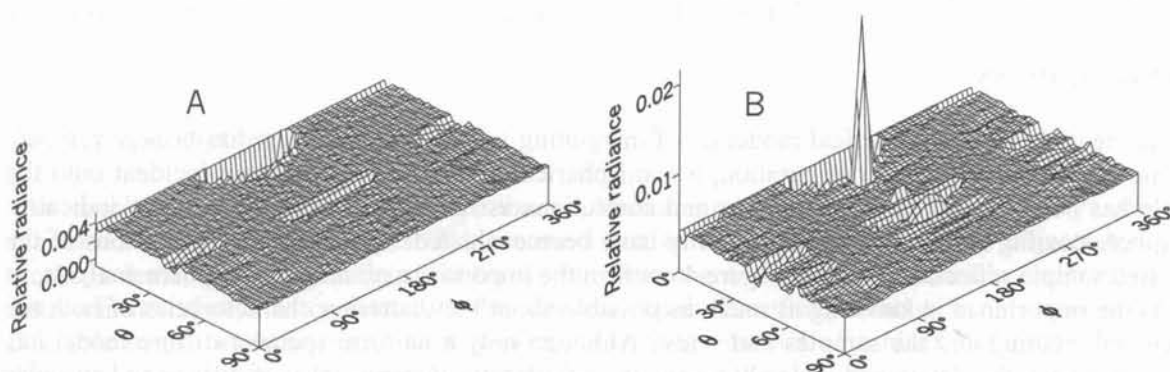


**Figure 3.** Angular distributions of relative radiance of light incident onto the sample center: A – sphere specularity 0.2; B – sphere specularity 0.4. In both cases the reflectances are 0.95.

Sphere non-uniformity can result in a systematic error that occurs for differing directional scattering character of the sample and reference reflection. This requires evaluation, and, if possible, correction. The most evident effect is the difference in loss through the exit port, which represents approximately 1.5% of the sphere wall area. In Figures 4A and B, plots of the calculated sample reflectance versus sample and sphere wall specularity, respectively, are shown for several values of sphere wall reflectance. In all cases the sample reflectance is 0.95, and the specularity  $S = 1$  in 4B. For each point in Figure 4,  $10^7$  rays were traced 10 times to find the mean reflectance factor value and its standard deviation  $\sigma$ . For most points,  $0.0005 < \sigma < 0.0015$ .

In the purely diffuse sphere wall case of Figure 4A, the deviation of the measured value from the real one (0.95) for sphere wall reflectance values of 0.95, 0.98 and 0.99 are shown to be linearly dependent on the sample specularity. The error in the measured sample reflectance is a combination of the exit port loss and the higher radiance level for the specular direction in comparison to the mean radiance (as can be seen in Figure 2B). The error is larger for lower wall reflectance because the radiance non-uniformity increases with decreasing wall reflectance.

The complicated dependence of measured sample reflectance on sphere wall specularity seen in Figure 4B, is determined by several effects that vary in strength as wall specularity is increased.

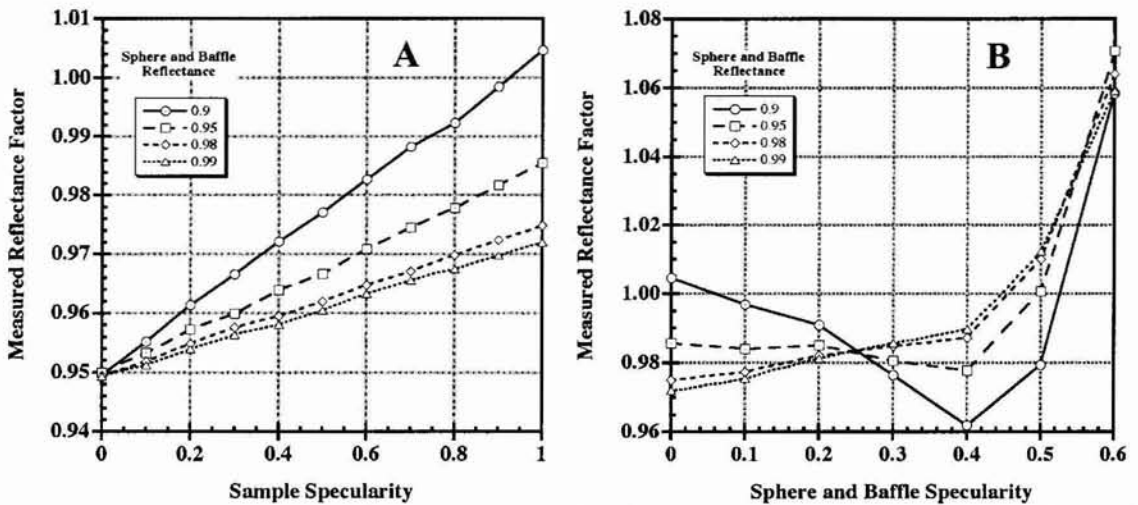


**Figure 4.** Measured sample reflectance as a function of (A) sample specularity and (B) sphere and baffle specularity for different values of sphere wall reflectance. In (B) the sample  $\rho = 0.95$  and  $S = 1$ .

## 5. CONCLUSIONS

A software code for the numerical modeling of integrating sphere reflectometers has been developed. For one important practical configuration, a hemispherical distribution of radiance incident onto the sample has been computed. Uncertainties and corrections associated with the light source indicatrix and sphere coating reflectance and specularity have been evaluated. The size of the deviations of the measured sample reflectance seen in Figure 4 confirm the importance of integrating sphere analysis, as well as the importance in knowing as much as possible about the scattering characteristics of both the sphere wall coating and the samples under test. Although only a uniform specular-diffuse model has been used so far, the developed code allows the use of arbitrary dependencies of diffuse and specular components on incidence angle. If a physically plausible algorithm for arbitrary BRDF sampling is made available, the code can easily be modified to add the capability of modeling such surfaces. A fast and reliable ray tracing technique has been developed that allows modeling of various integrating sphere-based reflectometers/emissometers for opaque and transparent materials, as well as for the optimization of extended uniform-radiance calibration light sources that use integrating spheres.

The authors would like to thank the Air Force Metrology Calibration Program, Engineering Division (AFMETCAL-MLE) for their support.

## REFERENCES

1. Kaplan S.G. and Hanssen L.M., *Proc. SPIE*, 1998, **3425**, 120-125
2. Battuello M., Ricolfi T. *High Temperatures-High Pressures*, 1989, **21**, 303-309
3. Clarke F., Compton J.J., *Color Res. Appl.*, 1986, **11**, 253-262
4. Hanssen L., Kaplan S., Mekhontsev S. – See *Proceedings of this Conference*
5. Hanssen L., *Applied Optics*, 1996, **35**, 3597-3606
6. Crowther B.G., *Applied Optics*, 1996, **35**, 5880-5886
7. Prokhorov A.V., Sapritsky V.I., Mekhontsev S.N., *Proc. SPIE*, 1996, **2815**, 118-125
8. Ziegler A., Hess H., Schimpl H., *Optik*, 1996, **101**, 130-136

## Address of the Authors:

Optical Technology Division, 100 Bureau Drive, Stop 8442, National Institute for Standards and Technology, Gaithersburg, MD 20899-8442, USA. E-mail: Leonard.Hanssen@nist.gov